Effect of precursor stoichiometry on morphology, phase purity, and texture formation of hot filament CVD diamond films grown on Si (100) substrate

Raju Ahmed[1] · Anwar Siddique[1] · Rony Saha[1] · Jonathan Anderson[1] · Chris Engdahl[2] · Mark Holtz[1,3] · Edwin Piner[1,3]

Abstract

The effect of precursor stoichiometry is reported on morphology, phase purity, and texture formation of polycrystalline diamond films. The diamond films were deposited on 100-mm Si (100) substrates using hot filament chemical vapor deposition at substrate temperature 720–750 °C using a mixture of methane and hydrogen. The gas mixture was varied with methane concentrations 1.5% to 4.5%. Diamond film thickness and average grain size both increase with increasing methane concentration. Diamond quality was checked using surface and cross-section by ultraviolet micro-Raman spectroscopy. The data show consistent diamond properties across the surface of the film and along the cross-section. XRD pole figure analyses of the films show that 3.0% methane results in preferential orientation of diamond in the $\langle 111 \rangle$ direction, whereas films deposited with 4.5% methane showed texture along the $\langle 220 \rangle$ direction in addition to $\langle 111 \rangle$ which was tilted ~23° with respect to the surface normal.

1 Introduction

Polycrystalline diamond thin films grown by chemical vapor deposition (CVD) are of interest, based on diverse properties, for various applications. Properties and applications include as a semiconductor for electronics, as a physically robust material for microelectromechanical systems (MEMS), and high thermal conductivity for use as a heat-spreading layer in power electronics [1–4]. For example, the possible power density in RF amplifiers, such as GaN-based high electron mobility transistors (HEMTs), increased by a factor of ~3 when diamond is employed as a substrate material to function as a passive heat spreader [5–8].

Diamond growth via hot filament CVD (HFCVD) involves dissociation of methane (CH_4) in the presence of energetic hydrogen atoms activated by the high filament temperature in a low-chamber pressure (5–100 torr) [9, 10]. The effects of various growth parameters, such as concentration of CH_4 in H_2, chamber pressure, substrate temperature, and filament to substrate distance, have significant effects on the structural and electronic properties of deposited diamond films.

CVD diamond properties are highly dependent on structure [11]. Polycrystalline orientation, grain size, surface roughness, and non-diamond carbon (NDC) percentage are some of the most important factors affecting the electrical and thermal properties of diamond films [2, 12, 13]. These factors, in turn, significantly affect CVD diamond's electrical and thermal properties [14].

Polycrystalline materials having completely random orientation are said to have no texture. When the crystallographic orientations are not random, but exhibit instead a preferred orientation, then the film is deemed textured. Depending on the percentage of preferred orientation, the film can be categorized as having weak, moderate, or strong texture along that direction [15]. Prior work has shown that formation of preferential orientation (textured) and grain formation in CVD diamond films are tunable by changing

✉ Edwin Piner
  epiner@txstate.edu

1   Materials Science, Engineering and Commercialization Program, Texas State University, San Marcos, TX 78666, USA

2   Crystallume Inc, 3397 De La Cruz Boulevard, Santa Clara, CA 95054, USA

3   Department of Physics, Texas State University, San Marcos, TX 78666, USA

growth parameters and growth duration [14]. Several groups have reported the effect of gas stoichiometry and process parameters on morphology and diamond quality [16–18], including the effect of oxygen during growth [19, 20]. Yang et al. [21] reported lower gas pressure resulting in the preferred formation of $\langle 110 \rangle$ textured diamond. Anaya et al. [13] demonstrated the effect of grain size and crystallographic orientation of CVD diamond on its thermal conductivity. Tang et al. [4] reported deposition of very smooth and highly $\langle 100 \rangle$ textured diamond film without any substrate bias in microwave plasma CVD using a gas mixture of $CH_4/H_2/O_2/N_2$. Liu et al. [14] demonstrated that the methane concentration in hydrogen has one of the most significant effects on forming highly $\langle 110 \rangle$ textured CVD films. However, we find no report studying the effects of constituent gas stoichiometry on morphology, quality and texture formation of CVD diamond [16].

Since morphology, phase purity, and crystallographic orientation of the diamond film is highly dependent on growth parameters, we investigate the effect of gas stoichiometry on morphology, phase purity, and crystallographic orientation in HFCVD films. We focus on these physical properties via Raman spectroscopy and X-ray diffraction.

2 Experimental details

To achieve high diamond nucleation density and process uniformity, nano diamond seeding was performed on 100-mm Si (100) wafers using spin coating. This process results in good cross-wafer seeding uniformity without damage to the substrate. Details about the seeding process can be found elsewhere [5, 6]. The resulting seed density is $10^{11}–10^{12}$ cm^{-2}. Substrate wafers, with the seed-laden resist in place, were loaded into a HFCVD system (Crystallume, Inc.) with 9 tungsten wires having 0.25 mm diameter and separation of 1 cm. The peak power drawn by the filament

array was maintained at 6 kW which resulted in a filament temperature of 2200 °C. A 6 mm filament-substrate separation results in uniform diamond growth with a substrate temperature of 720–750 °C [22]. An InGaAs-based optical pyrometer (Omega OS4000), with spectral response of 1.2 to 2.6 μm (suitable for viewing through quartz window), was used to measure the substrate surface temperature during the CVD diamond deposition. In our experiments, the methane concentration was varied from 1.5 to 4.5% (with corresponding CH_4 flow rates of 30 to 90 sccm) while keeping the H_2 flow rate at 2000 sccm. A small amount of O_2 (3 sccm) was also flowed into the chamber to maintain a low sp^2-bonded carbon concentration in the deposited films [23]. The HFCVD chamber pressure was kept at 20 Torr for all experiments. Initially, three diamond films were grown with 1.5, 3.0, and 4.5% CH_4 in H_2, respectively, while keeping the deposition time constant (8 h). Since each sample had different diamond thickness, we also grew samples at 1.5 and 4.5% CH_4 to approximately match the thickness of the 3.0% sample. These are discussed later. All samples studied are summarized, along with several key characteristics, in Table 1.

Morphology and thickness of the films were characterized using scanning electron microscopy (SEM, FEI Helios 400), atomic force microscopy (AFM, Bruker Dimension ICON) and surface profilometer (Dektak XT). Because the AFM images do not differ substantially from the SEM, we report only the root-mean-square (RMS) roughness R_q from AFM. To check diamond phase purity and quality across the thickness of the diamond film, micro-Raman measurements were conducted with ultraviolet (UV) excitation wavelength 363.8 nm. At this excitation wavelength, the diamond fluorescence is substantially lower than when measuring in the standard visible-wavelength range [24]. A laser line focus [25] was implemented and the collected light imaged at the charge-coupled device (CCD) detector following dispersal by the Raman spectrometer. Spectra

Table 1 Summary of morphology and diamond quality of diamond wafers deposited with three CH_4 concentrations

CH_4/H_2 (%)	Thickness (μm)	Average grain size (μm)	RMS roughness (nm)	Raman plan-view			Raman cross-section		
				O(Γ) peak shift (cm^{-1})	O(Γ) FWHM (cm^{-1})	$I_D/(I_D+I_{NDC})$	O(Γ) shift (cm^{-1})	O(Γ) FWHM (cm^{-1})	$I_D/(I_D+I_{NDC})$
1.5 (8 h)	1.1 ± 0.1	0.30 ± 0.05	87	1.65 (0.30)	4.1 (0.4)	0.5 (0.1)	-	-	-
3.0 (8 h)	3.9 ± 0.2	1.26 ± 0.26	163	0.85 (0.43)	7.8 (2.1)	0.2 (0.1)	0.70 ± 0.2	7.6 ± 0.5	0.3 ± 0.1
4.5 (8 h)	11.0 ± 0.3	1.59 ± 0.28	187	0.53 (0.30)	8.0 (0.8)	0.1 (<0.1)	0.5 ± 0.4	8.5 ± 1.2	0.1 ± 0.0
1.5 (20 h)	3.4 ± 0.1	0.92 ± 0.11	139	1.5 ± 0.1*	5.5 ± 0.1*				
4.5 (4 h)	4.0 ± 0.2	1.17 ± 0.25	133	1.6 ± 0.1*	8.6 ± 0.1*				

Data for the cross-section correspond to the topmost 0.25 μm of the diamond layer for comparison with the plan-view results. Values in parentheses correspond to standard deviations as discussed in the text

* From visible Raman data

collected in this mode generate a 400×1340 pixels image using a CCD detector with the long (1340) array axis corresponding to the Raman shift and the short (400) axis the line focus direction, approximately 10 µm long with a ×100 objective (NA 0.40). This approach simultaneously maps diamond properties across a diamond surface or cross-section in a single acquisition. Values obtained from these measurements are reported as averages along the line focus along with standard deviations. Details of the Raman line scan can be found elsewhere [6]. Visible micro-Raman spectra, not shown here, were measured using a Horiba (LabRAM) system (wavelength $\lambda = 532$ nm) with nominal spot diameter ~ 2 µm, utilizing a ×100 objective lens with NA 0.90. In all cases, spectra were collected to capture both the silicon and diamond O(Γ)-symmetry phonon lines and the NDC peaks in the 1450–1600 cm^{-1} range. Because the results from the visible Raman data are used to cross-check the UV Raman results, we include only the latter here. A natural diamond sample was used for obtaining a reference spectrum [6].

X-ray diffraction (SmartLab 3 kW XRD system, Rigaku Corporation) measurements were employed to analyze the crystal structure and the texture formation with Cu Kα radiation ($\lambda = 1.540562$ Å). Based on the wide angle θ–2θ XRD scan results, pole figure measurements were performed around diamond (111) and (220) peaks because of their relatively higher intensities. Pole figure data were collected using the Schulz method combined with a parallel beam [26]. Each pole figure was measured at a fixed scattering angle (2θ) and was obtained by a series of β (or φ) scans (azimuthal rotation around the normal to the surface of the sample by 0 to 360°) at different tilt angles (α or χ), between 0 to 90° with a step size of 3°. Pole densities were plotted in stereographic projection with obtained diffracted intensity data as a function of polar and azimuthal angles, χ and φ, respectively.

3 Results and discussion

3.1 Morphology and thickness

Figure 1(a–c) show representative plan-view SEM images of diamond films after 8 h growth. The insets are corresponding cross-section SEM images obtained by cleaving the wafers with no additional preparation. Excellent uniformity across the wafer in terms of diamond coalescence was achieved for all methane concentrations (CH$_4$:H$_2$ = 1.5%, 3.0%, and 4.5%). Grain structure variations were strongly correlated to methane concentrations. Film thickness and average grain size of the films are shown in Table 1. It is seen that grain size and film thickness vary greatly as a function of methane concentration. A 3.0% increase in methane concentration, from 1.5 to 4.5%, resulted in a film thickness increase from ~ 1 to ~ 11 µm for an identical 8 h growth time. The accompanying grain size increase was from ~ 300 nm to ~ 1600 nm. Thus, the nominal growth rates of CVD diamond films are ~ 140 nm/h, ~ 500 nm/h, and ~ 1400 nm/h for 1.5%, 3.0%, and 4.5% methane concentrations, respectively. The trend in growth rate is readily attributed to methane concentration based on availability of activated radicals [20]. Additionally, diamond growth in certain crystallographic facets are faster than in other facets [27–34]. These factors combine to result in thickness and grain size that follow the methane concentration [16, 17].

As seen in Fig. 1, diamond grains with apparently random shapes and relatively small sizes were observed for 1.5% methane and well faceted pyramid shaped polycrystals were visible in the case of 3.0% methane. Further increasing the methane concentration to 4.5% resulted in films with very large grains, but grains exhibited damage which can be attributed to etching by atomic hydrogen. To understand the etching, it is necessary to consider the chemical reactions that take place during diamond deposition. During the
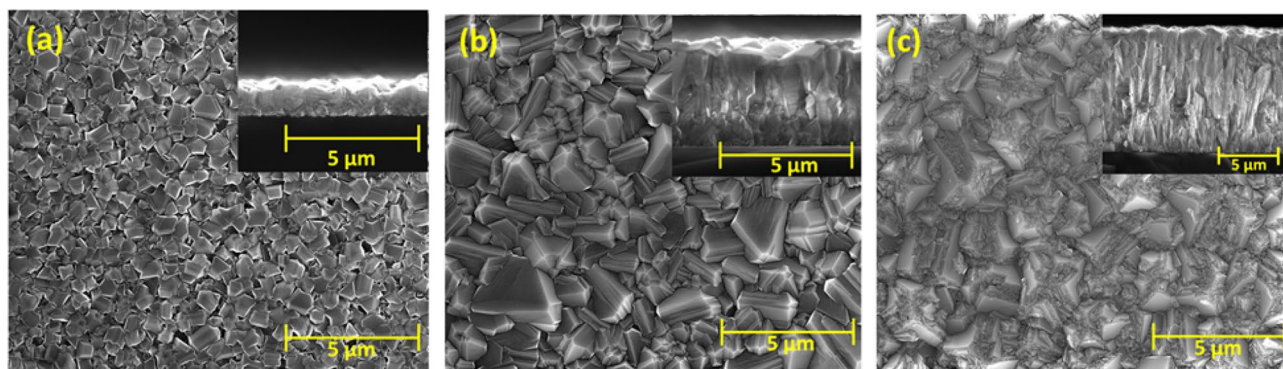
Fig. 1 SEM micrographs of diamond films deposited for 8 h with **a** 1.5%, **b** 3.0%, and **c** 4.5% methane in hydrogen. The insets are the corresponding cleaved cross-section SEM images

HFCVD process, clusters of carbon atoms are formed on the nano diamond seeded substrate surface. Heat causes a sequence of changes in the chemical bond structure from sp^1 to sp^2 and, eventually, sp^3 [35]. For HFCVD, the intentionally supplied oxygen provides energetic OH^- radicals that assists the atomic hydrogen to favorably remove sp^2-bonded carbon at the growth surface [23]. Therefore, the diamond deposition takes place with simultaneous etching of sp^2 carbon and formation of sp^3 [23]. The observed enhanced etching/damage on some crystal faces in the 4.5% methane sample can be a result of etch resistance of one face to another due to the presence of hydrogen at elevated temperature.

The observed increase in grain size with increasing methane concentration is a result of increased methyl radicals, which are the main source of carbon for diamond growth. Another model for explaining increased growth rate and grain formation with increasing methane concentration was reported by Jeon et al. [36] which claims that the majority of diamond nuclei clusters become negatively charged due to electrons originated from the hot filament. Clusters formed with lower methane concentration have low energy and higher methane concentration have higher energy. As a result, any increase in methane concentration enhances surface diffusion which assists in transforming cluster masses into well faceted diamond crystals. The decrease in grain size when diamond is deposited with methane concentration above 3.0% was reported by Ali et al. [16]. In their study, highly faceted diamond crystals were achieved with a methane concentration of 3.0%, while smaller crystals with pyramidal shape diamond clusters were achieved when the methane concentration was above 3.0%.

The cross-section SEM images, insets in Fig. 1(a–c), show that diamond crystals are very dense in the initial growth stage and a columnar-like growth continues as the film thickness increases. From grain size and grain boundary points of view, diamond quality improves as the film thickens post-coalescence and grains grow vertically [37]. Methane concentration strongly correlates with the non-diamond carbon phase concentration as we now discuss.

3.2 Raman spectroscopy

UV Raman spectra of diamond films, grown for 8 h, are shown in Fig. 2. Two sharp peaks are identified as Si O(Γ) (not shown) and diamond O(Γ) located at respective nominal reference energies $\omega_0 \sim 520$ and 1332 cm^{-1}. The peak shift is quantified using $\Delta\omega = \omega - \omega_0$ with ω_0 obtained at the time of each measurement to achieve best precision in $\Delta\omega$. The reference diamond linewidth is 4.8 cm^{-1}. The Raman-related numbers in Table 1 are average values obtained by binning spectra along the image direction. The bins correspond to ~ 0.25 µm segments along the 10-µm-long line focus, i.e., close to the diffraction limit dimension.
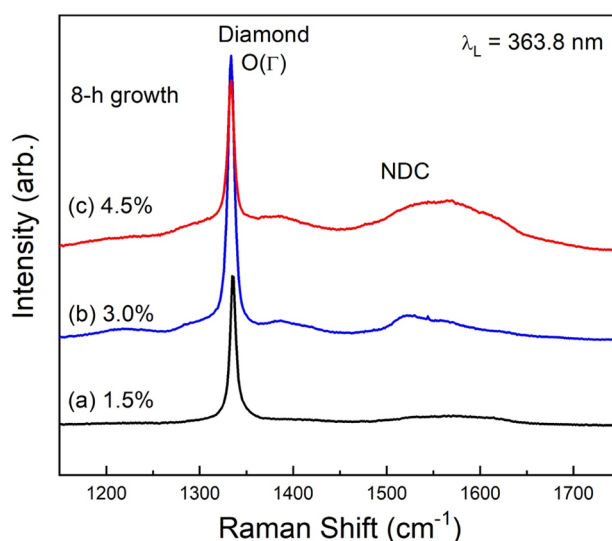
Fig. 2 UV (363.8 nm) Raman spectra of CVD diamond films deposited with 1.5, 3.0, and 4.5% methane grown for 8 h

Quantities in parentheses are standard deviations, rather than the small < 0.1 cm^{-1} uncertainty in position and width from fitting individual spectra. The standard deviations are informative to gain a better notion of diamond uniformity along the line focus. Variations along the line focus, and hence the standard deviations, are a consequence of the polycrystalline structure in the diamond film that locally affect stress and phase purity.

The observed blue-shift is attributed to compressive internal stresses in the diamond film. From the plan-view data, we see that blue-shift (compressive stress) in the thin diamond film is high and attributable to the differences in thermal expansion coefficient of diamond with the thick silicon substrate. The observed shift is consistent with silicon substrate-induced stress in our prior work [6]. As the diamond film thickness increases, the Raman measurement probes close to the top surface and we see smaller blue-shift, corresponding to relaxed stress. We return to this, following discussion of the diamond phase purity, with the micro-Raman cross-section.

The broad band centered at ~ 1550 cm^{-1} is due to the presence of various non-diamond carbon (NDC) phases and was observed in all diamond films studied. The NDC may be composed of disordered carbon having mixed sp^2 and sp^3 bonding configuration [38] and is considered to be undesirable for obtaining high thermal conductivity. Figure 2 shows that the intensity of the NDC peak increases as the percentage of methane increases. Qualitative information on diamond volume fraction in these samples can be obtained from the ratio of integrated intensities (area under curve after background correction) of diamond peak (I_D) to the total intensity I_D plus that from the non-diamond-like

carbon (I_{NDC}) [39]. The intensity ratio, $I_D/(I_D + I_{NDC})$, which does not correspond to diamond volume fraction, is low on account of the broad Raman band of NDC. Table 1 shows the change in this intensity ratio with methane concentration. We see the $I_D/(I_D + I_{NDC})$ ratio is highest at 1.5% methane concentration and decreases for 3.0% and 4.5% for the 8-h growth. The higher NDC, or lower $I_D/(I_D + I_{NDC})$, for higher methane concentration can be a result of increased formation of sp^2-bonded carbon when more methyl radicals are available in the CVD chamber to produce faster growth. The increase in NDC phase with increasing methane concentration is in agreement with previous reports [9, 23, 40].

CVD diamond properties generally vary between the initial growth nucleation and the coalescence regimes [41]. To examine the diamond quality along the growth direction, we performed cross-section UV micro-Raman line analysis on the samples grown with 3.0% and 4.5% methane, each of which had thickness suitable for these measurements. As mentioned above, the 3.0% methane sample had relatively high diamond phase based on the NDC intensity. The analysis of diamond phase purity was performed across the film thickness and the results are shown in Table 1.

To compare the cross-section to the plan-view, we bin pixels in the position direction of the CCD detector corresponding to averaging segments ~ 0.25 μm in length. For the plan-view analysis we followed the same 0.25 μm binning procedure. The 0.25 μm is close to the diffraction limit for our micro-Raman optics and this binning has the benefit of providing better signal to noise ratio for fitting. It also corresponds to the topmost region of diamond for direct comparison between plan-view and cross-section data. Results are summarized in Table 1. The plan-view and cross-section Raman data (of the top 0.25 μm) are consistent for the samples studied (3.0 and 4.5%) using both measurements. From the cross-section, shifts in the diamond peak position are slightly higher at the diamond/silicon interface, as expected. Moreover, we do not find a substantial change in the NDC intensity along the growth direction in either of these two samples.

3.3 XRD θ–2θ and pole figure

Measured θ–2θ XRD of the three samples are shown in Fig. 3. Three major diamond peaks, indexed as (111), (220), and (311) per ICDD card 06–675 [42], were visible at 43.9°, 75.3° and 91.5°, respectively. Other peaks are attributed to the Si (100) substrate (no beta filter was used for the scan). Peak positions vary slightly between samples due to thickness variation and compressive stress [12, 43]. It is well known that compressive stress in diamond film decreases as film thickness increases [44, 45]. The relative intensity of diamond (111) and (220) peaks changed significantly as the methane concentration was increased. Specifically, the
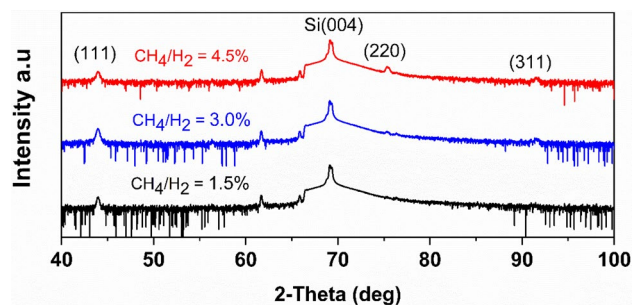
Fig. 3 X-ray diffraction spectra from CVD diamond films deposited with 1.5, 3.0, and 4.5% methane grown for 8 h

intensity of the diamond (111) peak was highest for diamond film grown with 3.0% methane, whereas the intensity of the diamond (220) peak was highest for film grown with 4.5% methane. For 1.5% methane, the intensity of the diamond (111) peak was affected by the reduced thickness. It is clear from Fig. 3 that diamond grown with 4.5% methane exhibits reduced integrated intensity of the (111) peak compared to that of the (220). This result suggests that diamond grown with 4.5% methane may have a preferential orientation toward (220), whereas for 3.0% there may be a preference toward (111). We note that such a comparison may also be affected by film thickness.

To better understand the effect of stoichiometry on texture in our CVD diamond, we performed pole figure analyses of these samples. Pole figure data from these experiments are used for observing qualitative differences in texture in CVD diamond films due to the change in gas stoichiometry. A detailed analysis on inverse pole figure and orientation distribution function of CVD diamond are not discussed in this manuscript and such analysis can be found elsewhere [14, 26, 46–48].

In pole figure data, reflection of the substrate is always visible for thin film samples because continuous Bremsstrahlung radiation happens to satisfy the diffraction condition. Therefore, very high intensity peaks from the Si substrate are present in all pole figures presented. Furthermore, a one-dimension (1D) detector was used for pole figure measurement which has an array of detectors and can capture a 2θ spread of ~ 3°. The sample grown with 1.5% methane did not show evidence of texture, due to substantially lower thickness. Therefore, the pole figure data from 3.0 and 4.5% methane samples are given here.

Pole figure data of the diamond (111) and (220) planes are shown in Fig. 4a and b, respectively, for the sample grown with 3.0% methane. Very high intensity peaks from Si (220) were visible in Fig. 4a because its Bragg angle of 47.63° is within 3.74° of the diamond (111) reflection. In the case of the diamond (220) pole figure shown in Fig. 4b, Si (004) and (331) peaks are present because the Bragg angle

Fig. 4 3D projection with relative pole figure intensity of **a** diamond (111) peaks and **b** diamond (220) peaks for the film grown with 3.0% methane for 8 h
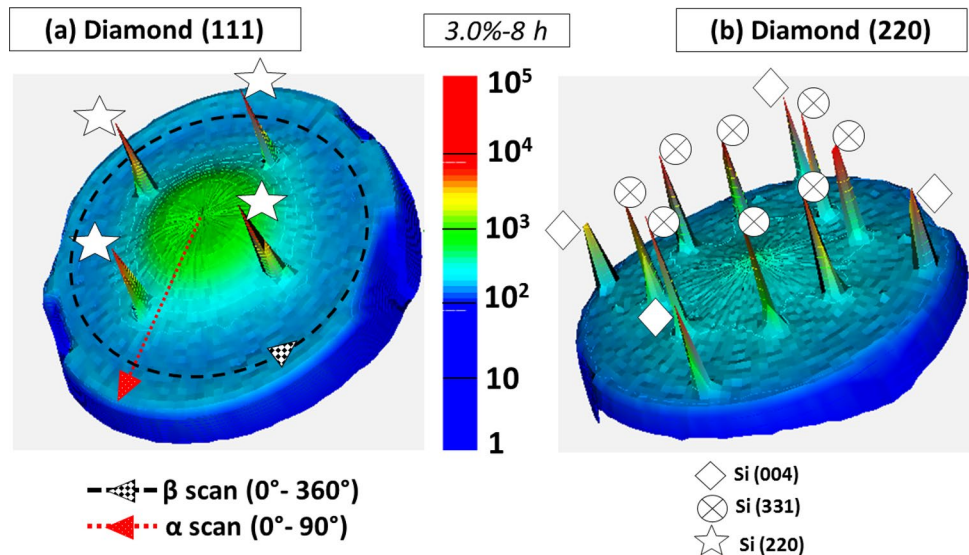
for Si (331) reflection is within 0.5° of diamond (220) [13]. In general, a strong texture in diamond along a certain direction is identified by a sharper peak centered at χ (or α) = 0°. Other peaks between χ = 0° and 90° represents tilting of a plane with its surface normal to the substrate [26].

Based on this general convention it is clear from Fig. 4a and b that diamond grown with 3.0% methane has very strong texture along $\langle 111 \rangle$ and the surface normal for (111) plane is nearly parallel to the surface normal of the substrate Si (100). On the other hand, no texture along $\langle 220 \rangle$ was seen for this sample. Texture formation in CVD grown polycrystalline diamond films have been reported and similar pole figure data for diamond (111) and (220) reflections have been observed in most of those cases [46, 49].

Clear texture formation was seen for both (111) and (220) reflections of diamond when methane concentration was 4.5% (not shown here). However, the (111) orientation is tilted ~45° with the surface normal for this sample. As discussed previously, the thicknesses of these samples were substantially different (see Fig. 1) and strong texture may

correlate with film thickness. Therefore, these results were insufficient to draw a definite conclusion about dependence of texture formation on methane concentration.

To conduct a more complete comparison of the effect of methane concentration for identical films, we subsequently grew samples with 1.5% and 4.5% methane with thicknesses close to 4 µm for direct comparison with the 3.0% sample. To achieve the target 4 µm thickness, 1.5% methane was grown for 20 h and 4.5% methane for 4 h. The thicknesses of these films were measured to be 3.38 ± 0.10 µm and 3.97 ± 0.18 µm, respectively. Figure 5a and b shows SEM and cleaved cross-section images of the two diamond films. In both cases, large polycrystals are obtained. The visible Raman spectra collected from three identical samples, not shown, confirms that the sample grown with 4.5% methane has poorest quality diamond among all three flow rates studied based on the higher NDC intensity. This is consistent with the UV Raman data in Fig. 2. Sample grown with 3.0% methane had relatively better diamond quality along with faster growth rate, while the samples grown at 1.5% methane

Fig. 5 SEM micrographs of diamond films deposited with **a** 1.5% for 20 h and **b** 4.5% methane for 4 h. The insets are the corresponding cleaved cross-section SEM images showing near identical thickness
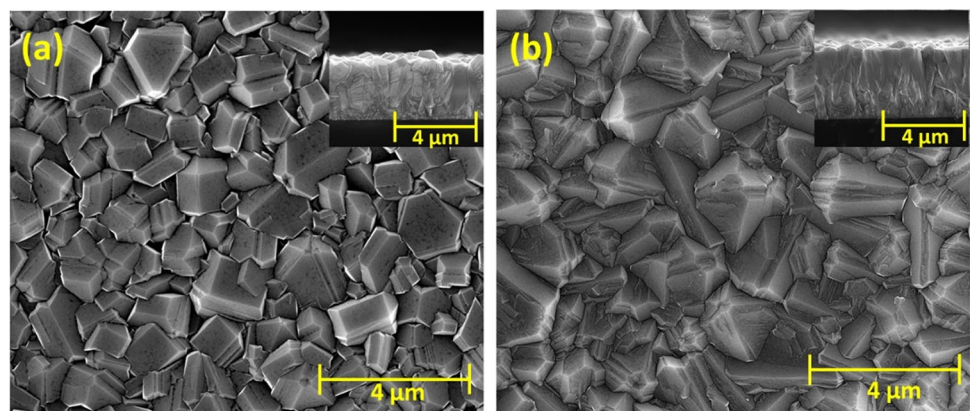
exhibited the narrowest diamond band. AFM images of three films with identical thickness, not shown, result in R_q values of 139, 163 and 133 nm for films grown with 1.5, 3.0 and 4.5% methane for 20, 8 and 4 h, respectively.

Pole figure data of the films with identical thickness show that the sample grown with 1.5% methane showed preferential orientation toward (111), the same as the 3.0% methane sample, but no texture toward (220) (not shown here). However, an interesting result was observed for the sample grown with 4.5% methane. The pole Fig. 3d projection images of the 4.5% methane sample are shown in Fig. 6a and b around the diamond (111) and (220) reflections, respectively. A preferred orientation toward ⟨111⟩ was observed for 4.5% methane, but with a tilt of ~23° relative to the surface normal. Furthermore, among all films, diamond with 4.5% methane showed a texture formation along ⟨220⟩, while no such preference was observed for 1.5 and 3.0% methane. Thus, the primary outcome of these pole figure data is that the increased methane concentration resulted in a texture formation along ⟨220⟩. Specifically, 4.5% methane resulted in preferential orientation in two planes, (111) and (220). The surface normal of (111) plane was tilted by ~23° with respect to the surface normal of the Si (001) substrate, while the surface normal of (220) plane was parallel to the surface normal of the Si (001) substrate. This indicates that with increasing methane concentration, the diamond films lose preferential orientation to a specific direction and results in more random orientation (textured in more than one crystallographic direction).

XRD in Fig. 3 show a relative decrease in the diamond (111) peak intensity compared to diamond (220) when the methane concentration was increased from 3.0 to 4.5%. The relative change in peak intensity has been reported as an indication of preferred orientation [14, 16, 21, 49]. Pole figures of the diamond (111) and (220) peaks shown in Fig. 4 and 6 indicate strong texture formation in films grown with 3.0% and 4.5% methane. A detailed description of texture formation in polycrystalline diamond is well understood and has been reported elsewhere [49, 50]. Since the goal of the present research is to perform a comparative analysis of preferred orientation as a function of gas stoichiometry, we restricted our analysis to pole figure data only. A detailed analysis of texture formation in CVD diamond films grown in similar condition is subject to future research. However, the current data will be explained based on a brief description of texture formation in polycrystalline diamond.

4 Discussion

A mechanism of texture formation in polycrystalline films during epitaxial growth was first proposed by Van der Drift [50] based on an evolutionary selection model of specific crystallite orientations. According to this model, randomly oriented nuclei grow freely and uniformly until they impinge on one another. Any given nucleus can prevail in the final film if its fastest growing crystallographic direction is perpendicular to the substrate, because such nuclei overgrow less favorably oriented ones. As a result, crystallographic texture forms in the film [14]. For polycrystalline diamond grown on Si (001), growth on nuclei facing parallel to the substrate are easily overgrown by crystals growing with the diagonal perpendicular to the substrate. Usually, growth rate along the diagonal plane (111) of a cubic crystal is $\sqrt{2}$ times that along the direction perpendicular to its face. Silva et al. [46] have also reported that the film texture is determined by the direction of the fastest growth corresponding to the largest dimension of the single crystal. As any polycrystalline

Fig. 6 3D projection of relative pole figure intensity of **a** diamond (111) peaks and **b** diamond (220) peaks for the film grown with 4.5% methane for 4 h
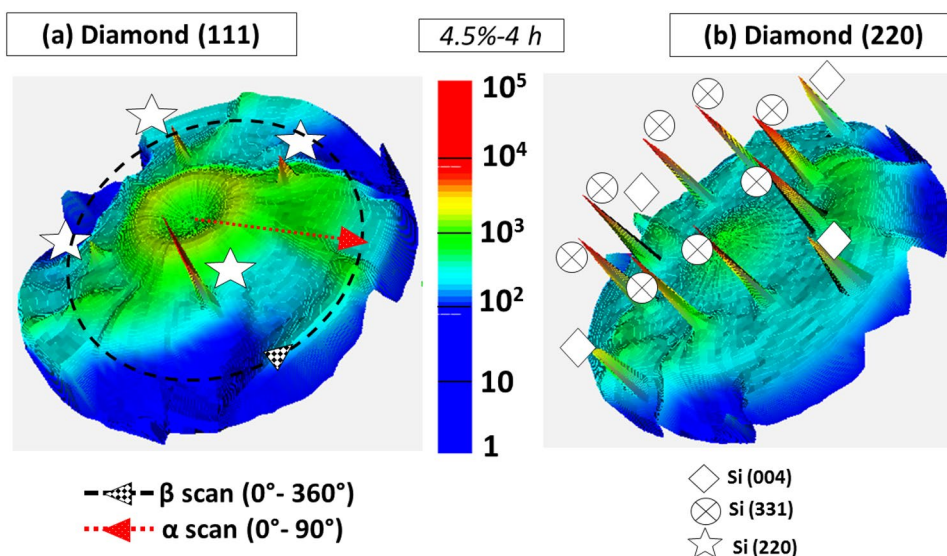
film thickens, more and more grains are buried by adjacent grains and crystals with the highest growth rate direction normal to the substrate are most likely to survive [46].

The largest dimension of isolated diamond crystal has been reported to be linked with the well-known α parameter, where $\alpha = \sqrt{3} \cdot V_{100}/V_{111}$ and V_{hkl} represents growth rate along the $\langle hkl \rangle$ direction [49]. The fastest growth direction in polycrystalline diamond changes from $\langle 111 \rangle$ to $\langle 110 \rangle$ to $\langle 100 \rangle$ when α is varied from 1 to 3, respectively. It is worth mentioning that the evolution selection model for texture formation is based on the assumptions of (1) no secondary nucleation and (2) the absence of crystallographic defects, such as twinning. However, in polycrystalline diamond, secondary nucleation and twinning readily occur. Due to secondary nucleation, nm-scale diamond grains exhibit elongated growth along the $\langle 110 \rangle$ direction after initial nucleation [46].

For CVD diamond, the growth rate of the (110) plane has been reported to be much faster than (111) and (100) when methane radicals were present in higher concentration in the CVD chamber [14, 21, 46]. The microstructure of CVD diamond films presented in Fig. 1 can be understood by a textured growth with an α value changing from ~ 1 to close to 1.5 (cuboctahedra as reported in [46]). While comparing morphology of diamond films with identical thickness in Fig. 5a, 1b and 5b, for 1.5, 3.0 and 4.5% methane, respectively, the morphology changed toward pyramidical shape. This morphology change is a combined result of secondary nucleation and the appearance of multi-twinned crystals having their largest dimension along a $\langle 110 \rangle$ axis. The effect of fastest growing $\langle 110 \rangle$ texture has been observed most clearly from the pole figure data of the 4.5% methane sample where, as seen from Fig. 6(b), texture along $\langle 220 \rangle$ seems to be surface normal but the texture along $\langle 111 \rangle$ showed ~ 23° tilt with the surface normal (the intense circle on Fig. 6a at ~ 23° from the center of the pole figure data). However, in the case of 1.5 and 3.0% methane, texture along the $\langle 111 \rangle$ plane was visible but no texture along $\langle 220 \rangle$ was visible. The morphology and pole figure results indicate that diamond grains are preferentially oriented toward the (111) plane until methane concentration is 3.0%. As the methane concentration increased to 4.5%, other planes, i.e., (220), appear and the film loses preferential orientation to any certain direction.

5 Conclusion

The effects of gas stoichiometry on morphology, quality, and crystal structure of HFCVD diamond have been studied. Higher growth rate and larger diamond grain size primarily results from the increased methyl radical concentration present in the chamber when methane concentration is increased. The volume fraction of sp^3-bonded diamond

was dictated by the methane concentration. Highest quality diamond (i.e., lowest NDC to diamond ratio) films were achieved with lower methane concentration (1.5%) but growth rate is relatively low. For higher methane concentration (4.5%), diamond phase purity was poorest, and it decreased even more as the film thickness increased. Diamond films grown with 3.0% methane showed higher growth rate and quality of diamond, comparable to 1.5% methane. Diamond films with pronounced texture were observed only when the thickness of the film was > 3 μm. Diamond films were found to be preferentially oriented along $\langle 111 \rangle$ direction when the methane concentration was 1.5–3.0%. In contrast, the sample grown with 4.5% methane showed texture along both $\langle 111 \rangle$ and $\langle 220 \rangle$ and the $\langle 111 \rangle$ texture showed ~ 23° tilt with the surface normal. Furthermore, the diamond phase volume fraction was lowest for this concentration. Secondary nucleation and twinning are proposed to be responsible for the observed high texture formation along $\langle 220 \rangle$ when methane concentration was high.

References

1. L. Yates, J. Anderson, X. Gu, C. Lee, T. Bai, M. Mecklenburg et al., low thermal boundary resistance interfaces for GaN-on-diamond devices. ACS Appl. Mater. Interfaces. **10**, 24302–24309 (2018)

2. O. Auciello, A.V. Sumant, Status review of the science and technology of ultrananocrystalline diamond (UNCD^{TM}) films and application to multifunctional devices. Diam. Relat. Mater. **19**, 699–718 (2010). https://doi.org/10.1016/j.diamond.2010.03.015

3. N. Heidrich, D. Iankov, J. Hees, W. Pletschen, R.E. Sah, L. Kirste et al., Enhanced mechanical performance of AlN/nanodiamond micro-resonators. J. Micromechanics Microengineering. **23**, 125017 (2013)

4. C.J. Tang, S.M.S. Pereira, A.J.S. Fernandes, A.J. Neves, J. Grácio, I.K. Bdikin et al., Synthesis and structural characterization of highly ⟨1 0 0⟩ -oriented {1 0 0}-faceted nanocrystalline diamond films by microwave plasma chemical vapor deposition. J. Cryst. Growth. **311**, 2258–2264 (2009). https://doi.org/10.1016/j.jcrysgro.2009.01.130

5. R. Ahmed, A. Siddique, J. Anderson, C. Engdahl, M. Holtz, E. Piner, Selective area deposition of hot filament CVD diamond on 100 mm MOCVD grown AlGaN/GaN wafers. Cryst. Growth Des. **19**, 672–677 (2019)

6. R. Ahmed, M. Nazari, B.L. Hancock, J. Simpson, C. Engdahl, E.L. Piner et al., Ultraviolet micro-Raman stress map of polycrystalline diamond grown selectively on silicon substrates using chemical vapor deposition. Appl. Phys. Lett. **112**, 181907 (2018)

7. G.H. Jessen, J.K. Gillespie, G.D. Via, A. Crespo, D. Langley, J. Wasserbauer, AlGaN/GaN HEMT on diamond technology demonstration, in *2006 IEEE Compd Semicond. Integr. Circuit Symp.*, 2006, p. 271–274

8. J.D. Blevins, G.D. Via, K. Sutherlin, S. Tetlak, B. Poling, R. Gilbert, et al., Recent progress in GaN-on-diamond device technology, in: Proc. CS MANTECH Conf, 2014, p. 105–108.

9. M.N.R. Ashfold, P.W. May, C.A. Rego, N.M. Everitt, Thin film diamond by chemical vapour deposition methods. Chem. Soc. Rev. **23**, 21–30 (1994)

10. J.E. Butler, Y.A. Mankelevich, A. Cheesman, J. Ma, M.N.R. Ashfold, Understanding the chemical vapor deposition of diamond: recent progress. J. Phys. Condens. Matter. **21**, 364201 (2009)

11. A. Siddique, R. Ahmed, J. Anderson, M. Nazari, L. Yates, S. Graham et al., Structure and interface analysis of diamond on an AlGaN/GaN HEMT utilizing an in situ SiN × interlayer grown by MOCVD. ACS Appl. Electron Mater **1**, 1387–1399 (2019)

12. J.J. Alcantar-Pena, J. Montes, M.J. Arellano-Jimenez, J.E.O. Aguilar, D. Berman-Mendoza, R. García et al., Low temperature hot filament chemical vapor deposition of Ultrananocrystalline Diamond films with tunable sheet resistance for electronic power devices. Diam. Relat. Mater. **69**, 207–213 (2016). https://doi.org/10.1016/j.diamond.2016.09.007

13. J. Anaya, T. Bai, Y. Wang, C. Li, M. Goorsky, T.L. Bougher et al., Simultaneous determination of the lattice thermal conductivity and grain/grain thermal resistance in polycrystalline diamond. Acta Mater. **139**, 215–225 (2017). https://doi.org/10.1016/j.actamat.2017.08.007

14. T. Liu, D. Raabe, W.-M. Mao, A review of crystallographic textures in chemical vapor-deposited diamond films. Front. Mater. Sci. China. **4**, 1–16 (2010)

15. H.-J. Bunge, *Texture Analysis in Materials Science: Mathematical Methods* (Elsevier, Amsterdam, 2013)

16. M. Ali, M. Ürgen, Surface morphology, growth rate and quality of diamond films synthesized in hot filament CVD system under various methane concentrations. Appl. Surf. Sci. **257**, 8420–8426 (2011). https://doi.org/10.1016/j.apsusc.2011.04.097

17. P. Mehta, R.E. Clausing, L. Heatherly, C.S. Feigerle, P.M. Menon, R.E. Clausing et al., The morphology of diamond grown by hot filament chemical vapor deposition. Diam. Relat. Mater. **7**, 1201–1206 (1998)

18. M.A. Taher, W.F. Schmidt, H.A. Naseem, W.D. Brown, A.P. Malshe, S. Nasrazadani, Effect of methane concentration on physical properties of diamond-coated cemented carbide tool inserts obtained by hot-filament chemical vapour deposition. J. Mater. Sci. **33**, 173–182 (1998)

19. Z.L. Tolt, L. Heatherly, R.E. Clausing, C.S. Feigerle, Hot filament assisted diamond growth at low temperatures with oxygen addition. J. Mater. Res. **12**, 1344–1350 (1997)

20. R. Beckmann, W. Kulisch, H.J. Frenck, R. Kassing, Influence of gas phase parameters on the deposition kinetics and morphology of thin diamond films deposited by HFCVD and MWCVD technique. Diam. Relat. Mater. **1**, 164–167 (1992)

21. S. Yang, Z. He, Q. Li, D. Zhu, J. Gong, Diamond films with preferred %3c110%3e texture by hot filament CVD at low pressure. Diam. Relat. Mater. **17**, 2075–2079 (2008). https://doi.org/10.1016/j.diamond.2008.07.005

22. J. Anderson, R. Ahmed, A. Siddique, E.L. Piner, HAADF-STEM study of filament material in hot filament CVD diamond films. Microsc. Microanal. **25**, 1788–1789 (2019)

23. P.W. May, Diamond thin films: a 21st-century material. Philos. Trans. R. Soc. Lond. A **358**, 473–495 (2000). https://doi.org/10.1098/rsta.2000.0542

24. M. Nazari, M.W. Holtz, Near-ultraviolet Raman and micro-Raman analysis of electronic materials. Appl. Phys. Rev. **5**, 41303 (2018)

25. K.A. Christensen, M.D. Morris, Hyperspectral Raman microscopic imaging using Powell lens line illumination. Appl. Spectrosc. **52**, 1145–1147 (1998). https://doi.org/10.1366/0003702981945138

26. K. Nagao, E. Kagami, X-ray thin film measurement techniques: VII Pole figure measurement. Rigaku J. **27**, 6–14 (2011)

27. C.J. Chu, M.P. d'Evelyn, R.H. Hauge, J.L. Margrave, Mechanism of diamond growth by chemical vapor deposition on diamond (100), (111), and (110) surfaces: carbon-13 studies. J. Appl. Phys. **70**, 1695–1705 (1991)

28. J.E. Butler, R.L. Woodin, Thin film diamond growth mechanisms. Phil. Trans. R. Soc. Lond. A. **342**, 209–224 (1993)

29. D. Huang, M. Frenklach, Energetics of surface reactions on (100) diamond plane. J. Phys. Chem. **96**, 1868–1875 (1992)

30. B.J. Garrison, E.J. Dawnkaski, D. Srivastava, D.W. Brenner, Molecular dynamics simulations of dimer opening on a diamond ${\$001\$}$(2x1) surface. Science **255**, 835–838 (1992)

31. S.J. Harris, Mechanism for diamond growth from methyl radicals. Appl. Phys. Lett. **56**, 2298–2300 (1990)

32. K. Larsson, S. Lunell, J.-O. Carlsson, Adsorption of hydrocarbons on a diamond (111) surface: an ab initio quantum-mechanical study. Phys. Rev. B. **48**, 2666 (1993)

33. T. Liu, D. Raabe, G. Eggeler, *High Resolution Investigation of Texture Formation Process in Diamond Films and the Related Macro-Stresses* (Ruhr-University Bochum, Bochum, 2009)

34. D. Kweon, J. Lee, D. Kim, The growth kinetics of diamond films deposited by hot-filament chemical vapor deposition. J. Appl. Phys. **69**, 8329–8335 (1991). https://doi.org/10.1063/1.347445

35. J. Singh, Nucleation and growth mechanism of diamond during hot-filament chemical vapour deposition. J. Mater. Sci. **29**, 2761–2766 (1994)

36. I.D. Jeon, C.J. Park, D.Y. Kim, N.M. Hwang, Effect of methane concentration on size of charged clusters in the hot filament diamond CVD process. J. Cryst. Growth. **223**, 6–14 (2001). https://doi.org/10.1016/S0022-0248(00)01016-2

37. R.B. Simon, J. Anaya, F. Faili, R. Balmer, G.T. Williams, D.J. Twitchen et al., Effect of grain size of polycrystalline diamond on its heat spreading properties. Appl. Phys. Express. **9**, 18–22 (2016). https://doi.org/10.7567/APEX.9.061302

38. S. Prawer, R.J. Nemanich, Raman spectroscopy of diamond and doped diamond. Philos. Trans. R. Soc. Lond. A **362**, 2537–2565 (2004)

39. M. Nazari, B.L. Hancock, J. Anderson, A. Savage, E.L. Piner, S. Graham et al., Near-ultraviolet micro-Raman study of diamond grown on GaN. Appl. Phys. Lett. **108**, 31901 (2016)

40. C.J. Tang, A.J.S. Fernandes, X.F. Jiang, J.L. Pinto, H. Ye, Effect of methane concentration in hydrogen plasma on hydrogen impurity incorporation in thick large-grained polycrystalline diamond films. J. Cryst. Growth. **426**, 221–227 (2015). https://doi.org/10.1016/j.jcrysgro.2015.06.018

41. M. Nazari, B.L. Hancock, J. Anderson, A. Savage, E.L. Piner, M. Holtz et al., Near-Ultraviolet micro-Raman study of diamond grown on GaN. Appl. Phys. Lett. **031901**, 31901 (2016). https://doi.org/10.1063/1.4940200

42. M.J. Fransen, J. te Nijenhuis, J.H.A. Vasterink, R.L. Stolk, J.J. Schermer, Analysis of the surface morphology of CVD-grown diamond films with X-ray diffraction. Adv. X-Ray Anal. **146**, 185–191 (2003)

43. A.C. Ferrari, J. Robertson, Interpretation of Raman spectra of disordered and amorphous carbon. Phys. Rev. B. **61**, 14095 (2000)

44. T. Guillemet, Z.Q. Xie, Y.S. Zhou, J.B. Park, A. Veillere, W. Xiong et al., Stress and phase purity analyses of diamond films deposited through laser-assisted combustion synthesis. ACS Appl. Mater. Interfaces. **3**, 4120–4125 (2011). https://doi.org/10.1021/am201010h

45. J. Michler, M. Mermoux, Y. Von Kaenel, A. Haouni, G. Lucazeau, E. Blank, Residual stress in diamond films : origins and modelling. Thin Solid Films **357**, 189–201 (1999)

46. F. Silva, F. Bénédic, P. Bruno, A. Gicquel, Formation of 〈110〉 texture during nanocrystalline diamond growth: a X-ray

diffraction study. Diam. Relat. Mater. **14**, 398–403 (2005). https://doi.org/10.1016/j.diamond.2004.11.019

47. T. Liu, D. Raabe, Growth rate and EBSD texture analysis of nitrogen doped diamond films, 2008. https://arxiv.org/abs/0812.4025.

48. K. Helming, S. Geier, M. Schreck, R. Hessmer, B. Stritzker, B. Rauschenbach, Texture analysis of chemical-vapor-deposited diamond films on silicon by the component method. J. Appl. Phys. **77**, 4765–4770 (1995)

49. C. Wild, P. Koidl, W. Müller-Sebert, Chemical vapour deposition and characterization of smooth {100}-faceted diamond films. Diam. Relat. **2**, 158–168 (1993). https://doi.org/10.1016/0925-9635(93)90047-6

50. A. der Drift, L.I.B. Rary, Evolutionary selection, a principle governing growth orientation in vapour-deposited layers. Philips Res. Rep. **22**, 267–288 (1967)